Intrinsic LINE-1 Hypomethylation and Decreased Brca1 Expression are Associated with DNA Repair Delay in Irradiated Thyroid Cells

Authors: Penha, Ricardo Cortez Cardoso, Lima, Sheila Coelho Soares, Boroni, Mariana, Ramalho-Oliveira, Renata, Viola, João P., et al.

Source: Radiation Research, 188(2) : 144-155

Published By: Radiation Research Society

URL: https://doi.org/10.1667/RR14532.1

RADIATION RESEARCH **188**, 144–155 (2017)
0033-7587/17 $15.00

DOI: 10.1667/RR14532.1

Intrinsic *LINE-1* Hypomethylation and Decreased *Brca1* Expression are Associated with DNA Repair Delay in Irradiated Thyroid Cells

Ricardo Cortez Cardoso Penha,[1,a] Sheila Coelho Soares Lima,[a] Mariana Boroni,[a] Renata Ramalho-Oliveira,[a] João P. Viola,[a] Denise Pires de Carvalho,[c] Alfredo Fusco[a,b] and Luis Felipe Ribeiro Pinto[a,2]

[a] *Instituto Nacional de Câncer - INCA, Rio de Janeiro, Brazil;* [b] *Istituto di Endocrinologia ed Oncologia Sperimentale - CNR c/o Dipartimento di Medicina Molecolare e Biotecnologie Mediche, Università degli Studi di Napoli ''Federico II'', Naples, Italy; and* [c] *Instituto de Biofisica Carlos Chagas Filho - CCS, Universidade Federal do Rio de Janeiro, Rio de Janeiro, Brazil*

Penha, R. C. C., Lima, S. C., Boroni, M., Ramalho-Oliveira, R., Viola, J. P., de Carvalho, D. P., Fusco, A. and Pinto, L. F. R. Intrinsic *LINE-1* Hypomethylation and Decreased *Brca1* Expression are Associated with DNA Repair Delay in Irradiated Thyroid Cells. *Radiat. Res.* 188, 144–155 (2017).

Exposure to ionizing radiation greatly increases the risk of developing papillary thyroid carcinoma (PTC), especially during childhood, mainly due to gradual inactivation of DNA repair genes and DNA damages. Recent molecular characterization of PTC revealed DNA methylation deregulation of several promoters of DNA repair genes. Thus, epigenetic silencing might be a plausible mechanism for the activity loss of tumor suppressor genes in radiation-induced thyroid tumors. Herein, we investigated the impact of ionizing radiation on global methylation and CpG islands within promoter regions of homologous recombination (HR) and non-homologous end joining (NHEJ) genes, as well as its effects on gene expression, using two well-established normal differentiated thyroid cell lines (FRTL5 and PCCL3). Our data reveal that X-ray exposure promoted G_2/M arrest in normal thyroid cell lines. The FRTL5 cells displayed a slower kinetics of double-strand breaks (DSB) repair and a lower long interspersed nuclear element-1 (*LINE-1*) methylation than the PCCL3 cells. Nevertheless, acute X-ray exposure does not alter the expression of genes involved in HR and NHEJ pathways, apart from the downregulation of *Brca1* in thyroid cells. On the other hand, HR and NHEJ gene expressions were upregulated in radiation-induced senescent thyroid cells. Taken together, these data suggest that FRTL5 cells intrinsically have less efficient DNA DSB repair machinery than PCCL3 cells, as well as genomic instability, which could predispose the FRTL5 cells to unrepaired DSB lesions and, therefore, gene mutations.

Editor's note. The online version of this article (DOI: 10.1667/RR14532.1) contains supplementary information that is available to all authorized users.

[1] Ricardo Cortez Cardoso Penha is ''Bolsista da CAPES, Programa PVE''.

[2] Address for correspondence: Instituto Nacional de Câncer - INCA, Rua André Cavalcanti, 37-Centro, Rio de Janeiro, CEP 20231-050 RJ, Brazil; email: lfrpinto@inca.gov.br.

INTRODUCTION

Thyroid carcinoma is the most frequently diagnosed malignancy of the endocrine system (*1*), and papillary thyroid carcinoma (PTC) accounts for approximately 80–85% of the cases (*2*). Exposure to ionizing radiation increases the risk of developing PTC, especially during childhood (*3*). Carcinogenic effects of radiation could be attributed to base damages, single-strand breaks and, above all, double-strand breaks (DSB), involved on *RET*/*PTC* rearrangement formation (*4*).

In response to DSB, a coordinated activation of sensors (γ-H2AX and 53BP-1), signal transducers and effectors, mostly homologous repair (HR) and non-homologous end joining (NHEJ) partners, is triggered (*5*). Defects in this machinery predispose to genomic instability and cancer (*6*).

Cancer arises from genetic and epigenetic alterations (*7*). Of these, CpG methylation is one of the most common mechanisms of gene expression regulation at the transcriptional level, usually associated with inactive chromatin when in the promoter region. Genomes from cancer cells simultaneously exhibit global hypomethylation and hypermethylation in promoters of specific tumor suppressor genes. These events frequently occur during the early stages of tumorigenesis (*7, 8*). The same phenomena have also been observed after radiation exposure (*9, 10*). Radiation could indirectly promote global hypomethylation and, therefore, genomic instability, a common feature observed in a variety of tumors, including PTC (*11*). On the other hand, hypermethylation of *MLH1* (*12*) and *ATM* (*13*) promoters has also been reported in PTC samples when compared to normal surrounding tissues and inversely associated with their expression and patient prognosis. Recent molecular characterization of PTC revealed a DNA methylation deregulation of several DNA repair gene promoters (*14*). Thus, early aberrant methylation of DNA repair genes could be a plausible mechanism of their silencing in radiation-induced thyroid tumors.

In this study, we investigated the effect of radiation on long interspersed nuclear element-1 (*LINE-1*) methylation, an

indicator of global methylation, and CpG islands within promoter regions of HR and NHEJ genes, as well as its effects on gene expression, using two well-established normal differentiated thyroid cell lines (FRTL5 and PCCL3). Our data reveal that FRTL5 displayed slower DSB repair kinetics and a lower *LINE-1* methylation than PCCL3 cells. Radiation did not appear to modify the expression of genes involved in HR and NHEJ pathways apart from the downregulation of *Brca1* in the thyroid cells. On the other hand, radiation-induced senescence promoted upregulation of HR and NHEJ gene expression in thyroid cells.

MATERIALS AND METHODS

Cell Culture and Irradiation

Rat thyroid cells, PCCL3 and FRTL5, derived from 18-month-old and 3–4-week-old normal Fisher rats, respectively (*15*), were grown in Coon's modified Ham's F-12 media (HiMedia Laboratories, Mumbai, India), supplemented with 5% fetal bovine serum and a six-hormone mixture [1 mU/ml thyrotropin (TSH), 10 μg/ml insulin, 5 μg/ml transferrin, 10 n*M* hydrocortisone, 10 ng/ml somatostatin and 10 ng/ml glycyl-L-histidyl-L-lysine acetate-complete media].

Acute irradiations were performed as single 1–10 Gy X-ray doses (X-RAD 320; Precision X-ray Inc., North Branford, CT) for 1–48 h. In parallel, 20 μm of H_2O_2 (Sigma-Aldrich® LLC, St. Louis, MO) was used as a positive control of water radiolysis (indirect effect of radiation) (*16*). Synchronization of 97% of FRTL5 cells on G_0/G_1-phase cell cycle was performed, as previously described by Degrassi *et al*. (*17*). Briefly, cells were starved from TSH for 72 h, then TSH was added to the media and cells were monitored for three days.

For chronic exposures, five X-ray treatments of 5 Gy were performed to reach a maximum dose of 25 Gy (X-RAD 320; Precision X-Ray) with intervals of two or three days between each treatment. This protocol was based on a childhood cancer cohort in which the estimated mean thyroid dose was 12.50 Gy (*18*).

Cytotoxicity and Cell Cycle

As an index of cell viability, we used the commercially available MTT assay (Sigma-Aldrich), according to the manufacturer's instructions. All measurements were performed in triplicate and the results were expressed as relative to nonirradiated control cells or irradiated cells at the initial time (1 h). Trypan blue was used to evaluate cell proliferation at 1, 6 and 24 h postirradiation.

Cell cycle profile was evaluated using propidium iodide (2 μg/ml) on a FACSCalibur™ cytometer (Becton Dickinson and Co., Franklin, NJ) and analyzed on CELL-FIT software (Becton Dickinson).

Western Blot

Cells were homogenized in lysis buffer containing 135 m*M* NaCl, 1 m*M* $MgCl_2$, 2.7 m*M* KCl, 20 m*M* Tris, pH 8.0, 1% Triton™, 10% glycerol and protease and phosphatase inhibitors (0.5 m*M* Na_3VO_4, 10 m*M* NaF, 1 m*M* leupeptin, 1 m*M* pepstatin, 1 m*M* okadaic acid and 0.2 m*M* phenylmethylsulfonyl fluoride) and then syringed five times. An aliquot was used to determine the protein concentration by BCA protein assay kit (Pierce™ Biotechnology/Thermo Fisher Scientific Inc., Rockford, IL), according to the manufacturer's instructions. Cell lysate proteins (30–100 μg) were then subjected to SDS/PAGE electrophoresis, transferred to polyvinylidene fluoride (PVDF) microporous membranes, and probed with the indicated antibodies: anti-γ-H2AX, 1:1,000 (EMD Millipore, Billerica, MA); anti-β-actin, 1:10,000 (Sigma-Aldrich); anti-BRCA1, 1:1,000 (Novus Biologicals, Oakville, Canada); anti-phospho-ATM, 1:2000 (Rockland); anti-ATR, 1:2,000 (Novus Biologicals); anti-Vinculin, 1:1,000 (Santa Cruz Biotechnology® Inc., Dallas, TX); anti-rabbit, 1:2,000 (Abcam, Cambridge, UK); anti-mouse, 1:3,000 (Santa Cruz Biotechnology); anti-goat, 1: 3,000 (SouthernBiotech, Birmingham, AL). The detection of the proteins was performed using ECL (Pierce Biotechnology/Thermo Fisher Scientific).

Immunofluorescence of γ-H2AX and 53BP-1

Irradiated and control cells were fixed in methanol-acetone solution (70:30) at –20°C for 7 min, permeabilized with 0.5% Triton X-100 solution for 30 min and dried. After rehydration in phosphate-buffered saline and blocking with 1% bovine serum albumin for 1 h, cells were stained with the anti-γ-H2AX (1:500; EMD Millipore) for 90 min and Alexa Fluor® 488 anti-mouse (1:250, Invitrogen™, Carlsbad, CA) as secondary antibody for 1 h. The same procedure was performed for 53BP1 (1:500; Novus Biologicals) with Alexa Fluor 594 anti-rabbit (1:250; Invitrogen). Nuclei were counterstained with 40,6-diamidino-2-phenylindole (DAPI). Coverslips were mounted using Vectashield® mounting media (Vector® Laboratories, Burlingame, CA). Fluorescence images were obtained using an Olympus FV10i confocal microscope (Olympus, Tokyo, Japan). To determine the average total number of foci per cell, per field, for three independent experiments, we counted the number of γ-H2AX foci per cell used NIH ImageJ software, v.38.

Pyrosequencing

Lesion-specific DNA repair pathway genes (HR and NHEJ), involved on DNA damage response, were selected due to CpG island presence on their promoter regions using UCSC Genome Browser (University of California, Santa Cruz, CA) (Table 1). To access the *LINE-1* methylation pattern of the cell line genomes, we used two sets of primers designed by Hamm *et al*. (*19*). We obtained the rat genome sequence (rn4/v. 3.4, November 2004) and annotation for repetitive elements from the UCSC Genome Database. Based on the provided data, 899,092 *LINE-1* sequences were subjected to *in silico* bisulfite treatment and 8,460 L1 elements with length over 6,000 bp were identified and aligned to generate LINE nucleotide base matrix. The sets of primers for pyrosequencing analysis were designed within L1 elements with dense CpG dinucleotides. An electronic PCR was performed and the consensus sequence was visualized using WebLogo (*20*). A total of 1,285 PCR products with 117 pb mean length were generated. The two sets of primers allowed us to assess 7 CpG dinucleotides within each L1 sequence, generating data from a minimum of 8,995 CpG sites. The DNA was eluted to reach a final concentration of 25 ng/μl. To quantify the percentage of methylated cytosines in individual CpG sites, bisulfite-converted DNA was sequenced using a pyrosequencing system (PSQTM 96MA, QIAGEN, Hilden, Germany), as previously described (*8*).

Real-Time PCR

A total of 1,500 ng of RNA was used in the reverse transcription reaction (RT) using SuperScript II® (Invitrogen), following the manufacturer's protocol. The oligonucleotides for real-time PCR, comprising exon-exon junctions, were purchased from Integrated DNA Technologies® (San Diego, CA), designed with Primer-BLAST software (National Center for Biotechnology Information, Bethesda, MD) and are listed in Table 2. We used the Rotor-Gene® Q system and QuantiFast® reagent SYBR Green PCR Kit (both from QIAGEN®, Valencia, CA). Each reaction contained 5 μl of QuantiFast SYBR Green buffer 2X (QIAGEN), 0.5 μl of specific oligonucleotides at a final concentration of 0.25 μ*M*, 3 μl of cDNA (diluted 10×) and sterile deionized water to complete the final volume of 10 μl. The amplification reaction was performed as follows: 5 min of predenaturation at 95°C, followed by 40 cycles of denaturation for 5 s at 95°C and an annealing and extension step for 10 s at 60°C. Relative gene expression was determined using comparative C_t method (*21*) and *RPL4* was used as a housekeeping gene.

TABLE 1
Pyrosequencing Primers Used in this Study Selected According to the Signaling Pathways

Signaling pathways	Genes	Region (CpG)	Sequences	Product (bp)	Sequence to analyze
HR	*Atm*	Promoter (80)	F: AGTAAAGAAGGGGTAAGAGG R: ACTCAAACTAAATTCTTCCTATA S: TTTGATGAGAATTTTTTTTTATAGA	267	AGTT**YG**AG**YG**TT**YG**TTTTT**YG**TTTTTAT
	Brca1	Promoter (23)	F: GGAGAGGAGGAGTAAGTTGA R: CTTCCACAATCCTCTATTTACC S: GTTATAGTAATTTTGTATAAAGGG	317	T**YG**GAAT**YG**TTATTTGAGGT**YG** GAATATGAG**YG**TAAGGTAGTGTTTA
	Mre11	Promoter (47)	F: AGGATTGGTTTTTGTGAGTTATT R: CCTAAATTACCCCAACCTAAACTTAT S: GTTATGTTATTATTGGT	232	TTT**YGYG**AGAAGTA**YG** GATG**YG**TTTTTTT**YGYG**TTTAATTTAGGTTT
	Rad50	Promoter (16/37)	F: GGGAAGTGGATGAAGTGGATGATTA R: TCTTCAACCCCCTCACAATTT S: TGGGTTAGGTTAGTTGA	203	GGTTTT**YG**AGGTTTA**YG**TATTATAAGG**YG**ATATTTTAAATATTTTTTGGGGTTT
	Xrcc1	Promoter (50)	F: AGGGGTTTTTTTAGGGAGGT R: CAAAACTCCCCTTTTTCCTTAC S: GGGATTTTGAGGGG	172	**YG**T**YGYG**GGTGGGGTTTTT**YG**AGGTTGGA
NHEJ	*Lig4*	Promoter (44)	F: GGTTGGATTGGGATTTATAGG R: TTCAAATACTTAAATCCAAACACACTCT S: GTTTAGGTAAGTAAAGTATTAATG	154	TAATAGGTA**YG**TAGGTTTATTT**YG**TTGAG**YG**TTTTTGAAAGTTTGTGATAAT
	Xrcc6	Promoter (66)	F: GGGTTAGGTTTTTGGATAGGT R: CTCTCTCTATCACCTCACAATAATC S: GGTTTTATTAGGAT	264	T**YG**TGG**YGGYG**GTTA**YG**ATGGTTTT**YG**GGTATT
	Xrcc4	Promoter (38)	F: AAGGGTGATGTGGTTGGATTAG R: ACTCTTCCTAAATCTATTAACCTAATACTC S: GGGGATGGTG	243	**YG**GG**YG**TTGTGGGG**YGYG**GGAGTTTTGGTTTTAGTGTGATTTT
Retrotransposon	*Line-1*	5′-UTR	F: TTGGTGAGTTTGGGATAT R: AAATCTAAAAACAAAAAACTACTAC S1: TAGAATTTTTTTAGGAT S2: ATAGGAAGTTTTATATT	117	S1: **YG**GGTA**YG**TTTTGTGTTTAT**YG**GAAGTT S2: **YGYG**GATTT**YG**GTT**YG**TAGTAG

Notes. This table encompasses: CpG island's length and region, sequence, PCR set of primers and the sequence analyzed by pyrosequencing. HR = homologous recombination repair; NHEJ = non-homologous end joining; retrotransposon = *LINE-1* (long interspersed nuclear element-1).

Beta-Galactosidase Activity

Total proteins of 2×10^5 cells were extracted using RIPA buffer (25 m*M* Tris-HCl pH 7.6, 150 m*M* NaCl, 1% NP-40, 0.1% SDS, 1% sodium deoxycholate, 50 m*M* NaF, 1 m*M* EDTA) and protease inhibitors (0.2 m*M* PMSF, 1 m*M* pepstatin and 80 m*M* aprotinin). Nonirradiated control and irradiated whole cell lysates (10 μl) were incubated with 40 μl of buffer Z (60 m*M* $Na_2HPO_4.7H_2O$, 40 m*M* $NaH_2PO_4.H_2O$, 10 m*M* KCl, 1 m*M* $MgSO_4.7H_2O$ and 0.3% 2-mercaptoethanol) containing 1 mg/ml X-Gal (Sigma-Aldrich) for 3 h (pH 7). Absorbance was measured at 595 nm.

TABLE 2
qPCR Primers Used in this Study Selected According to the Signaling Pathways

Signaling pathways	Gene	Sequences	Amplicon (bp)
HR	*Rad50*	F: 5′-GGCTGGGGAGGATGATTGAG-3′ R: 5′-TGCTTAGTTCACGTTCCGCT-3′	156
	Atm	F: 5′-GACATGCCAGGGTGAAGGAA-3′ R: 5′-TTTCCAGTTCTCCGACTGCC-3′	108
	Mre11	F: 5′-TCTGTACGGCTTAGGGTCCA-3′ R: 5′-TGAAGTTGGTGCTTCCGTGT-3′	155
	Brca1	F: 5′-CTGTGGTGAAGGAGCTTCCA-3′ R: 5′-CCCAATATCAGGGCAGTCGTT-3′	107
	Xrcc1	F: 5′-GGAACAGTCAGAAGGACGGG-3′ R: 5′-GAATTGGCAGGTCAGCCTCT-3′	191
NHEJ	*Lig4*	F: 5′-CAGGTTGCTTAGTTAAAACCGGAG-3′ R: 5′-GAGCACAAGTCTGCAAAGGG-3′	103
	Xrcc6	F: 5′-TTGGTCAACGGGAGCTCAAC-3′ R: 5′-GGGAGACATTCTTTCGGGCT-3′	103
	Xrcc4	F: 5′-GGAGACACCGAATGCAGACA-3′ R: 5′-GCCAAGCCTTTCCTTCTCCT-3′	86
L4E family of ribosomal proteins	*Rpl4*	F: 5′-GGCCTTCAGAAACATCCCTG-3′ R: 5′-CCATACAACTCATCCAACTTCCG-3′	138

Note. HR = homologous recombination repair; NHEJ = non-homologous end joining; L4E family of ribosomal proteins = housekeeping gene.

Statistical Analysis

All results were expressed as mean ± SD. Basal gene expression, global methylation, cell viability, cell cycle and β-galactosidase activity were analyzed by the nonparametric Kruskal-Wallis test followed by Dunnett's multiple comparison test. Data regarding promoter methylation, gene expression and γ-H2AX foci were analyzed by two-way analysis of variance (ANOVA) followed by Bonferroni post-hoc test. Statistical analyses were performed using Prism v. 5 (Graphpad Software Inc., San Diego) and differences were considered statistically significant at $P < 0.05$.

RESULTS

High X-Ray Doses do not Compromise Cell Viability and Promote G_2/M Arrest

To evaluate the effects of X rays on a normal thyrocyte cell cycle, FRTL5 and PCCL3 cells were X irradiated with 1–10 Gy or treated with 20 μM H_2O_2 (water radiolysis), and cell viability and cycle were evaluated (Fig. 1). Both cell lines remained viable after 48 h in all conditions (Fig. 1A and B). As expected, irradiation blocked cell proliferation up to 24 h (Fig. 1C and D). Cells were arrested in G_2/M phase, in a dose-dependent manner, at 24 h postirradiation compared to paired nonirradiated controls, and these events were earlier (12 vs. 24 h) and more pronounced in FRTL5 than PCCL3 after 10 Gy X-ray irradiation (PCCL3: 33% vs. 21%; FRTL5: 45% vs. 22%; $P < 0.05$) (Fig. 1E and F). In addition, exposure also diminished the percentage of cells in G_0/G_1 and S phases, with such proportions being normalized 48 h postirradiation, compared to their respective nonirradiated controls (Fig. 1E and F).

FRTL5 Cells Display a Slower Kinetics of DSB Repair than PCCL3

Since γ-H2AX and 53BP-1 are early DSB sensors (*5*), they were used as an indirect measure of DSB lesions. Both cell lines exhibited a peak of γ-H2AX at 1 h postirradiation, but PCCL3 restored control levels sooner than FRTL5 (6 vs. 12 h) (Fig. 2A and Supplementary Fig. S1; http://dx.doi.org/10.1667/RR14532.1.S1). No γ-H2AX signal was detected in PCCL3 cells at 6 h postirradiation (Supplementary Fig. S1) Accordingly, in FRTL5, γ-H2AX foci per cell reached the maximum number at 1 h postirradiation compared to the respective control (104 vs. 5), 68% repaired after 6 h (33 vs. 6), and the control levels were restored after 24 h, although few damage sites remained unrepaired (10 vs. 5) (Fig. 2). Interestingly, in PCCL3, a peak of γ-H2AX foci per cell was induced at 1 h postirradiation compared to the respective control (131 vs. 1) and the control levels were restored after 6 h (3 vs. 1) (Fig. 2). 53BP1 and γ-H2AX displayed similar expression kinetics with strong colocalization (Pearson's coefficient = 0.93) (Fig. 2C). Concerning upstream targets of the DSB-response pathway, radiation induced ATR expression and ATM (p-ATM) activation in both cell lines (Fig. 2D).

FRTL5 Cells Have Lower Basal LINE-1 Methylation than PCCL3

Since global hypomethylation is associated with genomic instability and DNA damage (*9*), we evaluated the *LINE-1* methylation profile of rat thyroid cells, an indirect indicator of global methylation (*22*), through the interrogation of seven CpG sites within a consensus region of L1 elements by pyrosequencing. Our data revealed that, compared to PCCL3, FRTL5 cells have lower *LINE-1* methylation levels (71.18 vs. 82.93%) and the latter levels were similar in different rat tissues (thyroid, breast, liver and kidney) (Fig. 3A). Surprisingly, exposure to 10 Gy did not have an effect on the *LINE-1* methylation profile of either thyroid cell line (Fig. 3C and E), even when 97% of the cells were synchronized in G_0/G_1 phase of cell cycle with TSH deprivation (Fig. 3B).

FRTL5 Cell Line Expresses Lower Basal Brca1 mRNA Levels than PC Cl3

We investigated the expression of DNA repair genes involved on DSB response pathways (HR and NHEJ). FRTL5 and PCCL3 cell lines showed different *Brca1* mRNA levels, which were more abundant in PCCL3 than FRTL5 cells (Fig. 4B). Conversely, no changes were observed in the expression of the other selected genes, such as *Atm*, *Rad50*, *Mre11*, *Xrcc1*, *Xrcc4*, *Xrcc6* and *Lig4* (Fig. 4A and C–H). Interestingly, DNA methylation levels of their CpG-rich promoters were null or low (0–6.5%) (Table 3).

Ionizing Radiation Affects Brca1 Expression Regardless of DNA Methylation of its Promoter Region on the FRTL5 Cell Line

We investigated whether radiation could influence DNA methylation and expression of DNA repair genes. Radiation induced a decrease of up to 50% of the *Brca1* mRNA and protein levels in FRTL5 cells compared to paired-controls (1, 6 and 24 h postirradiation) (Fig. 5A and C). In PCCL3 cells, the downregulation of *Brca1* (for approximately 50%), at protein level, was also observed during the first 6 h postirradiation (Fig. 5D), although no significant differences were found at mRNA levels (Fig. 5B). No modulation of the expression of the DNA repair genes (*Atm*, *Rad50*, *Mre11*, *Xrcc1*, *Xrcc4*, *Xrcc6* and *Lig4*) was observed, at least at the transcriptional level (Supplementary Fig. S2; http://dx.doi.org/10.1667/RR14532.1.S1). Moreover, the CpG sites within the promoter region of all the selected genes were not altered by radiation (Supplementary Table S1; http://dx.doi.org/10.1667/RR14532.1.S1), even when FRTL5 cells were synchronized at the G_0/G_1 phase of the cell cycle (Supplementary Table S2; http://dx.doi.org/10.1667/RR14532.1.S1). These results suggest that DNA methylation of the promoter region of HR and NHEJ genes is not influenced by radiation.

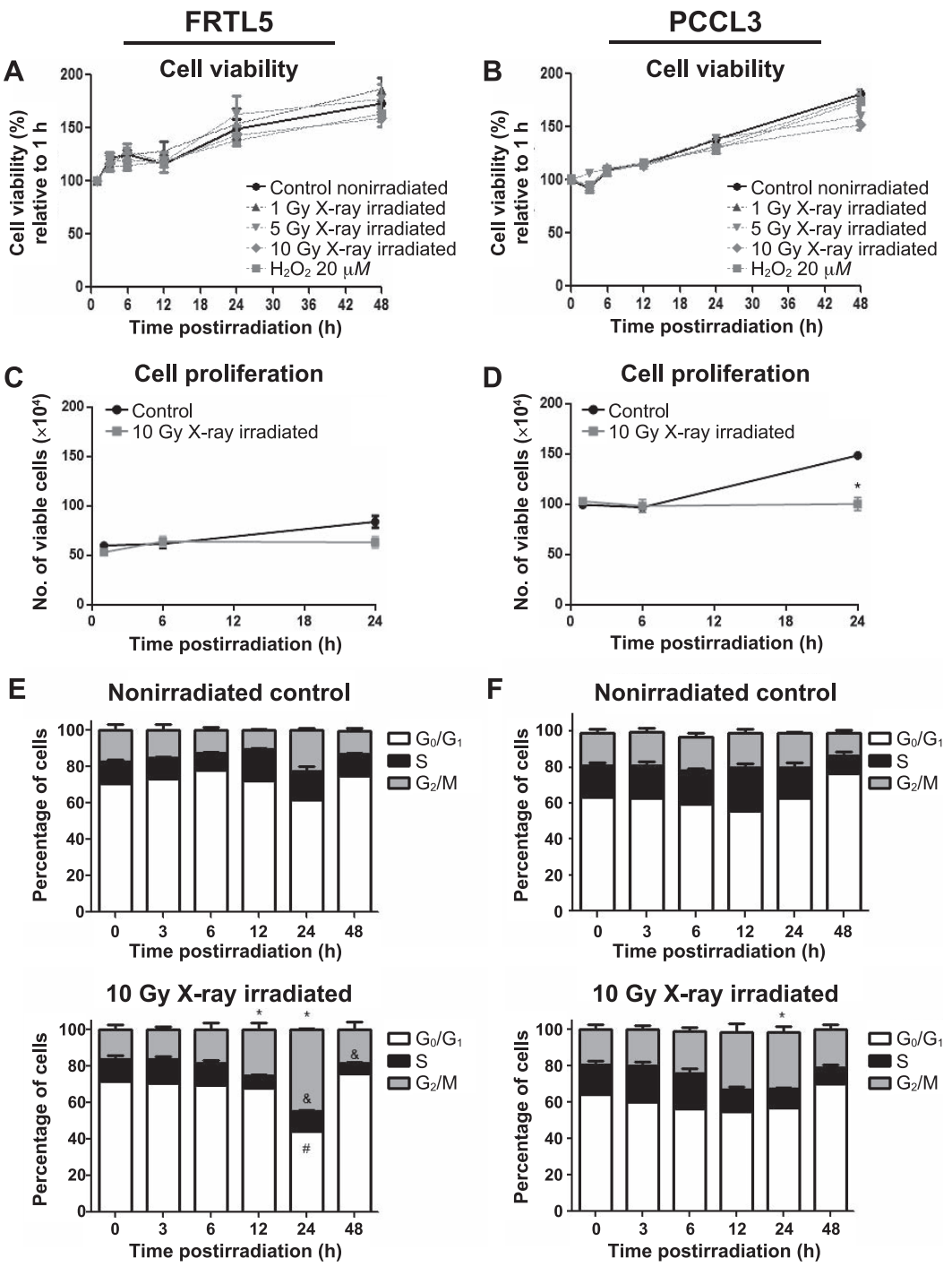

FIG. 1. Cytotoxicity and cell cycle profile of FRTL5 and PCCL3 cell lines after X-ray irradiation. FRTL5 and PCCL3 cell lines were X-ray irradiated with 1–10 Gy or treated with 20 μM H_2O_2 (water radiolysis), and cell viability and proliferation, as well as cell cycle, were evaluated. Panels A and B: Cell viability of FRTL5 and PCCL3, respectively. Panels C and D: Cell proliferation of FRTL5 and PCCL3, respectively. Panels E and F: Cell cycle of FRTL5 and PCCL3, respectively. All determinations were made in triplicates of three independent experiments and the results were expressed as: relative to nonirradiated control cells (black line) or irradiated in initial time (1 h) (dotted gray lines) for cell viability; number of viable cells ($\times 10^4$ cells) for cell proliferation; percentage of cells in G_0/G_1 (white bar), S (black bars) and G_2/M (gray bars) compared to their respective nonirradiated controls for each cell cycle. $^*P < 0.05$ compared to G_2/M phase for nonirradiated control; $^{\&}P < 0.05$ compared to S phase for nonirradiated control, $^{\#}P < 0.05$ compared to G_0/G_1 phase for nonirradiated control.

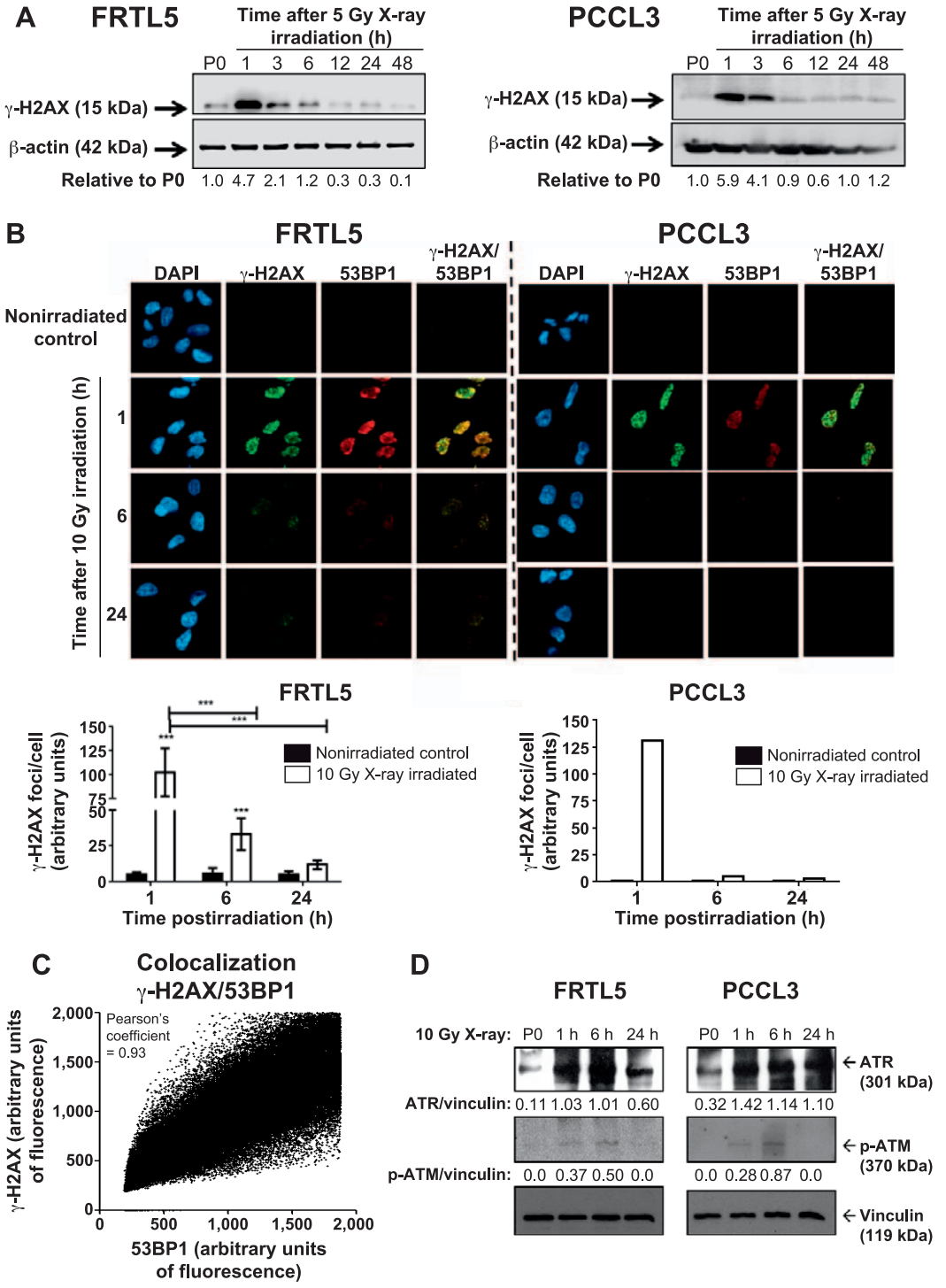

FIG. 2. Double-strand break (DSB) repair kinetics of FRTL5 and PCCL3 cells. Panel A: Representative γ-H2AX immunoblots of irradiated thyroid cells at 1–48 h postirradiation. Intensity quantification was relative to the starting point (0 h) (P0). Panel B: Immunofluorescence of nonirradiated control and irradiated FRTL5 and PCCL3 cells stained with anti-γ-H2AX (green) and 53BP1 (red). Nuclei were counterstained with DAPI (blue). In parallel, the number of γ-H2AX foci per cell was determined as an average of the total foci number per cell per field. Panel C: Foci colocalization of γ-H2AX and 53BP1. Panel D: Representative p-ATM and ATR immunoblots of irradiated thyroid cells at 1, 6 and 24 h postirradiation. Absolute intensity quantification was calculated as ratio target: vinculin. Beta-actin and vinculin were used as loading control. $***P < 0.001$ compared to nonirradiated control.

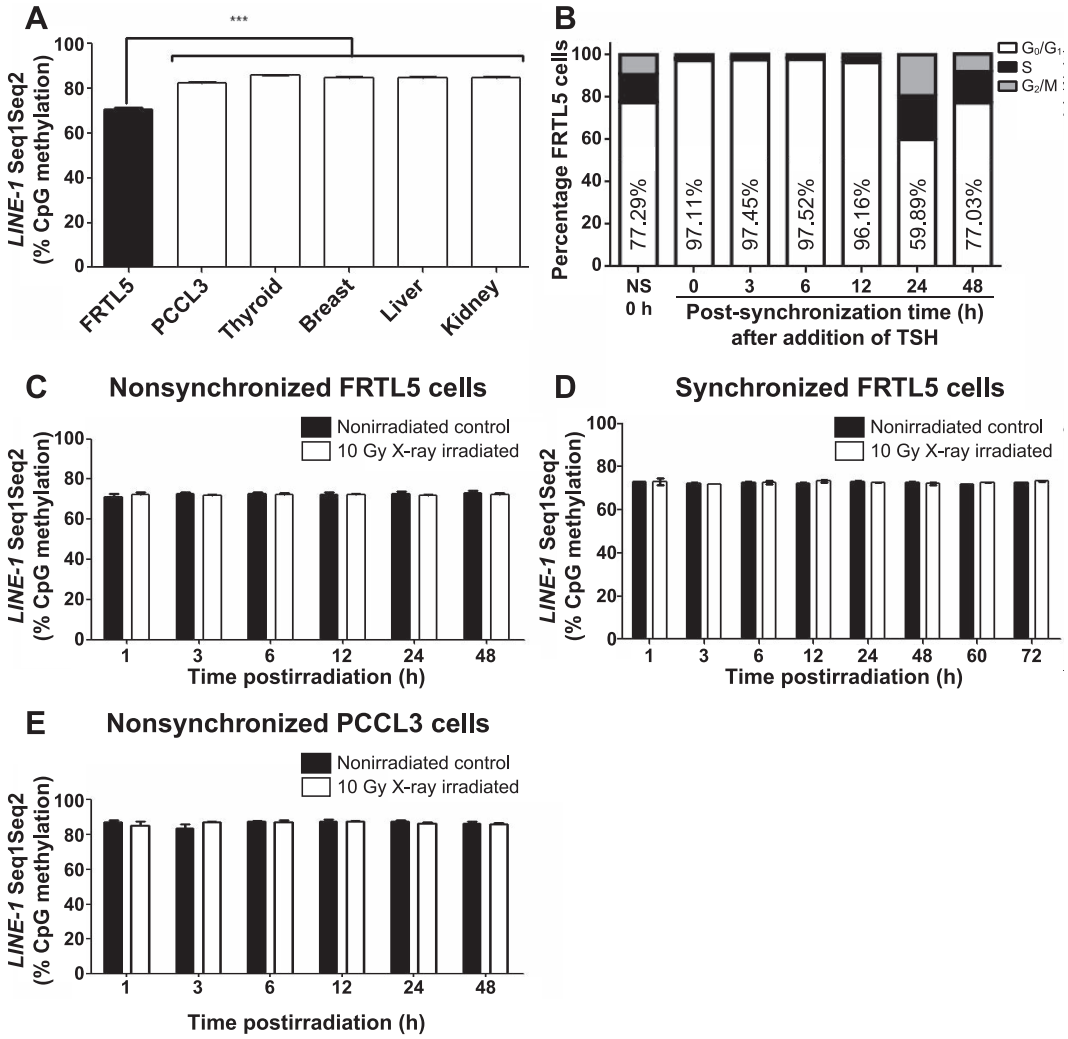

FIG. 3. Global methylation of thyroid cell lines. Panel A: *LINE-1* pyrosequencing of FRTL5 and PCCL3 cell lines. Rat tissues (thyroid, breast, liver and kidney) were used as control. Panel B: Synchronization of FRTL5 cells in G_0/G_1-phase cell cycle was performed by starving cells of thyrotropin (TSH) for 72 h, and then adding TSH to the media, after which the cells were monitored for three days. NS = nonsynchronized. Panels C–E: *LINE-1* pyrosequencing. Nonsynchronized and synchronized FRTL5 cell lines (panels C and D, respectively), and nonsynchronized PCCL3 cell lines (panel E) are shown for both nonirradiated paired control and 10 Gy X-ray irradiated cells. The results are expressed as percentage of cells that displayed methylation on seven selected CpG sites within L1 elements. $***P < 0.001$.

Chronic Exposure caused Senescent Phenotype to occur in FRTL5 Cells

We established a chronic exposure model with the FRTL5 cell line. Figure 6 shows that the number of viable irradiated cells reached a plateau after the second radiation treatment, while the number of viable paired nonirradiated control cells increased with time (Fig. 6A). Accordingly, radiation induced a gain in β-galactosidase activity (Fig. 6B) and promoted morphological changes (flattened, elongated and enlarged cell shape) (Fig. 6C), suggesting a radiation-inducible senescence phenotype. Moreover, no *LINE-1* methylation changes were observed in irradiated cells (Fig. 6D).

Chronic Radiation Exposure Promotes Upregulation of HR and NHEJ Genes in the FRTL5 Cell Line

When assessing the long-term effect of exposure on DNA repair gene expression, we observed an upregulation of all HR and NHEJ DNA repair genes, selected for this study, after the fifth radiation treatment (25 Gy) (Fig. 7). In addition, a transient increment of mRNA levels of *Brca1*, *Mre11*, *Xrcc1* and *Xrcc4* was also detected after the third radiation treatment (15 Gy) (Fig. 7B, D–F, H). These data indicate that radiation-induced senescence elicits an activation of HR and NHEJ genes in the FRTL5 cell line.

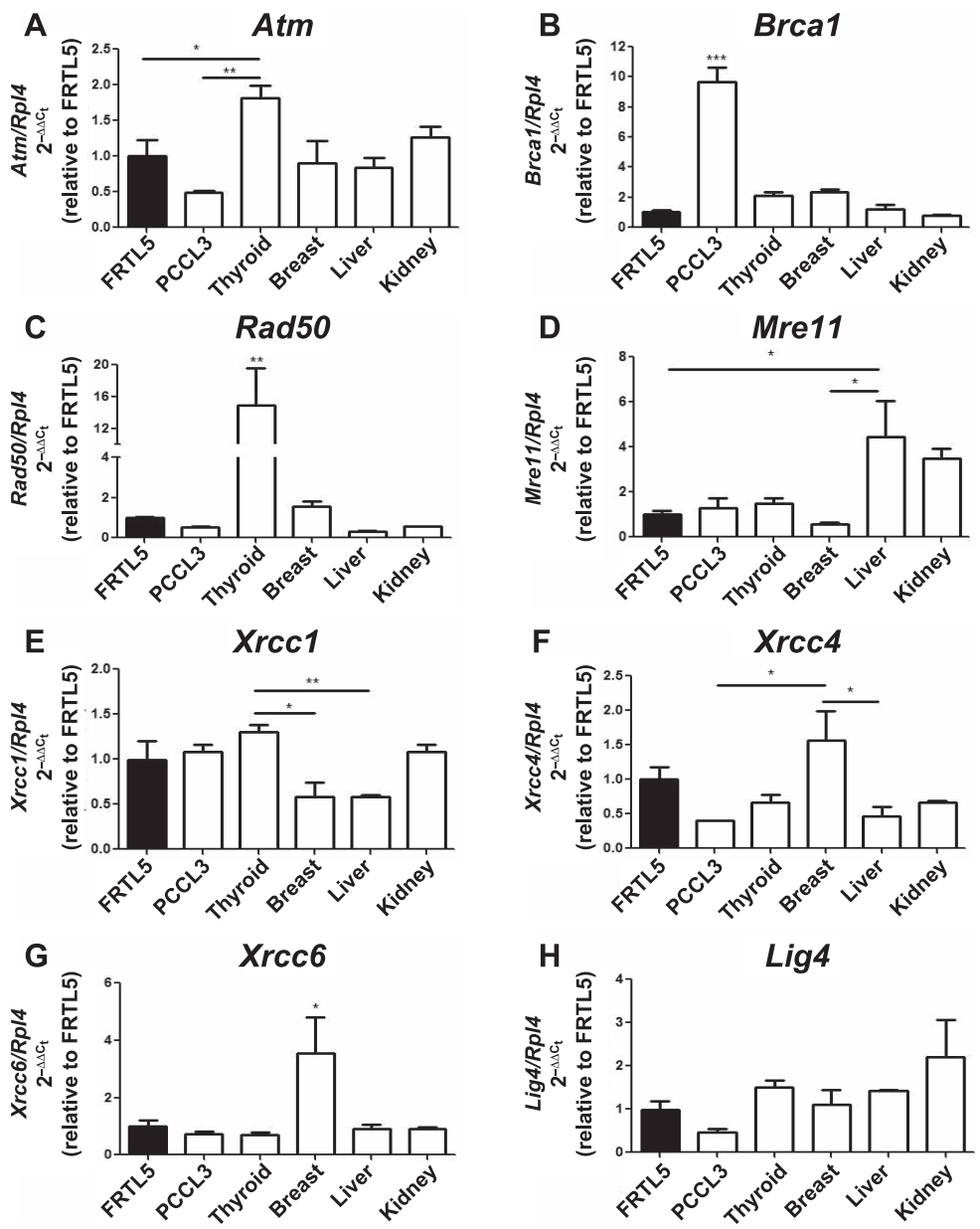

FIG. 4. Basal expression of double-strand break (DSB) genes in thyroid cell lines. Relative mRNA expression levels are shown according to DNA repair pathways of FRTL5 and PCCL3 cell lines: HR (panels A–E) and NHEJ (panels F–H). Expression levels are relative to the FRTL5 cell line. Rat tissues (thyroid, breast, liver and kidney) were used as control. $*P < 0.05$; $**P < 0.01$.

TABLE 3
Basal Promoter Methylation Profiles of HR and NHEJ Genes

	Percentage CpG methylation (average)							
	Atm	*Brca1*	*Rad50*	*Mre11*	*Xrcc1*	*Xrcc4*	*Xrcc6*	*Lig4*
FRTL5	0.00 ± 0.0	2.10 ± 2.1	1.05 ± 0.9	0.00 ± 0.0	4.36 ± 1.9	0.00 ± 0.0	0.61 ± 0.5	6.5 ± 0.5
PCCL3	2.59 ± 0.5	0.92 ± 0.9	0.44 ± 0.8	0.00 ± 0.0	0.95 ± 0.3	0.00 ± 0.0	3.08 ± 0.4	2.00 ± 0.0
Thyroid	1.31 ± 1.3	1.83 ± 0.4	3.88 ± 0.7	0.00 ± 0.0	1.09 ± 0.5	0.00 ± 0.0	0.00 ± 0.0	2.00 ± 0.0
Breast	0.00 ± 0.0	1.42 ± 1.3	2.66 ± 0.0	0.00 ± 0.0	1.03 ± 0.2	0.00 ± 0.0	0.44 ± 0.8	3.50 ± 1.5
Liver	0.00 ± 0.0	2.83 ± 1.1	2.11 ± 1.00	0.00 ± 0.0	0.75 ± 0.3	0.00 ± 0.0	0.50 ± 0.9	2.17 ± 0.3
Kidney	1.57 ± 2.7	1.75 ± 0.3	3.11 ± 1.3	0.00 ± 0.0	0.98 ± 0.5	0.00 ± 0.0	0.00 ± 0.0	4.50 ± 0.9

Notes. Pyrosequencing of HR (*Atm*, *Brca1*, *Rad50*, *Mre11 and Xrcc1*) and NHEJ genes (*Xrcc4*, *Xrcc6 and Lig4*) were performed on nonexposed thyroid cell lines (FRTL5 and PCCL3) and rat tissues (thyroid, breast, liver and kidney). The results were expressed as percentage of cells that displayed methylation on selected CpG sites ±SD.

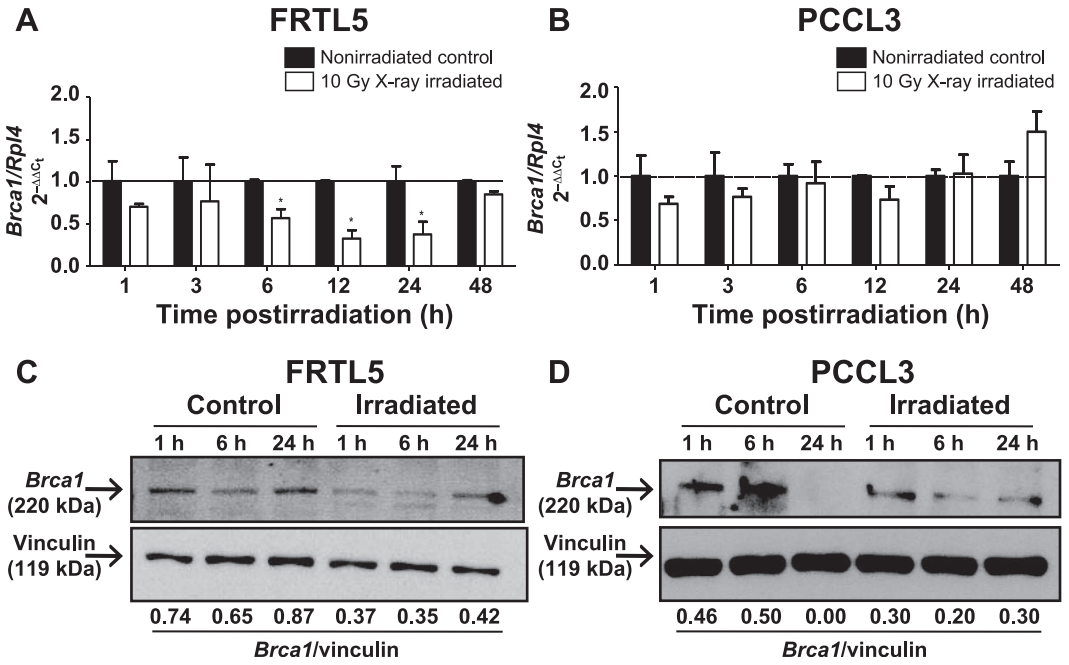

FIG. 5. Expression of *Brca1* gene after acute 10 Gy X-ray irradiation in FRTL5 and PCCL3 cell lines. Cells were irradiated (white bars) and *Brca1* mRNA levels evaluated in FRTL5 and PCCl3 cell lines (panels A and B, respectively). Expression levels were relative to paired nonirradiated controls (black bars). Representative *Brca1* immunoblots are shown for irradiated FRTL5 and PCCL3 thyroid cells (panels C and D, respectively) at 1, 6 and 24 h postirradiation. Vinculin was used a loading control. Absolute intensity quantification was calculated as ratio *Brca1*/vinculin. $*P < 0.05$.

DISCUSSION

In this study, we demonstrate that radiation exposure promotes G_2/M arrest in two differentiated thyroid cell lines, in agreement with what has been previously reported by Green *et al*. (*23*), using the FRTL5 cell line. However, radiation-induced cell cycle arrest was more pronounced in the FRTL5 than PCCL3 cell line, which may be explained by the higher proliferation rate of FRTL5 (*24*) with respect to PCCL3. Our data also reveal that normal rat thyroid cells respond quickly to radiation insults, and repair them within a few hours, in agreement with previously reported results in human primary thyrocytes (*25*). Therefore, FRTL5 and PCCL3 are potentially suitable models for elucidating DNA repair in the thyroid. Above all, FRTL5 cells repaired radiation-induced DSB later than PCCL3 and, as a result, these cells are prone to accumulate DNA damages.

As for upstream targets of the DSB-response pathway, the expression of ATR and p-ATM revealed significant differences in the capacity for DNA repair between these two cell lines. In PCCL3 cells, ATM phosphorylation was much higher than FRTL5 cells at 6 h postirradiation, while ATR expression was higher in FRTL5 than PCCL3 cells at 1–6 h postirradiation. These kinases play an essential role in the maintenance of genomic integrity as well as act as barriers during early tumorigenesis (*26*). Interestingly, even though ATM and ATR share some downstream effectors, they are activated in response to different types of lesions (*26*). While ATM is primarily involved in double-strand break pathways, ATR responds to a broader spectrum of DNA damages, especially those that interfere with DNA replication. Thus, these data could be linked to the delayed DSB repair in FRTL5 cells and to the differential *Brca1* expression in the thyroid cell lines.

Our findings also demonstrate that FRTL5 cells have a lower *LINE-1* methylation level compared to PCCL3 and thyroid tissue. *LINE-1* methylation levels have been widely used as a surrogate marker for global methylation status in cancer, not only due to the abundancy of such elements, but also due to its ability to distinguish normal tissue from tumor tissue (*22*). In addition, it has been shown that decreased *LINE-1* methylation levels can already be observed in early stages of tumor development (*27*) and associated with an increased risk of cancer development (*28*). Global hypomethylation is commonly related to genomic instability and transformation of normal cells into cancer cells (*9, 29*), and is also crucial in thyroid cancer progression (*11*). Therefore, FRTL5 cells appear to be more susceptible to genomic instability and malignant transformation than PCCL3 cells, as previously reported (*15*). Since radiation was not capable of modulating *LINE-1* methylation levels in FRTL5 and PCCL3 cells, even when cells were synchronized, we could hypothesize a protective mechanism was in place to maintain cell viability. In fact, treatment with the demethylating agent 5-aza-2′-deoxycytidine compromises human thyroid cancer cell viability (*30*). Interestingly, FRTL5 cells express lower *Brca1* levels than PCCL3, and irradiation caused a drastic decrease in the

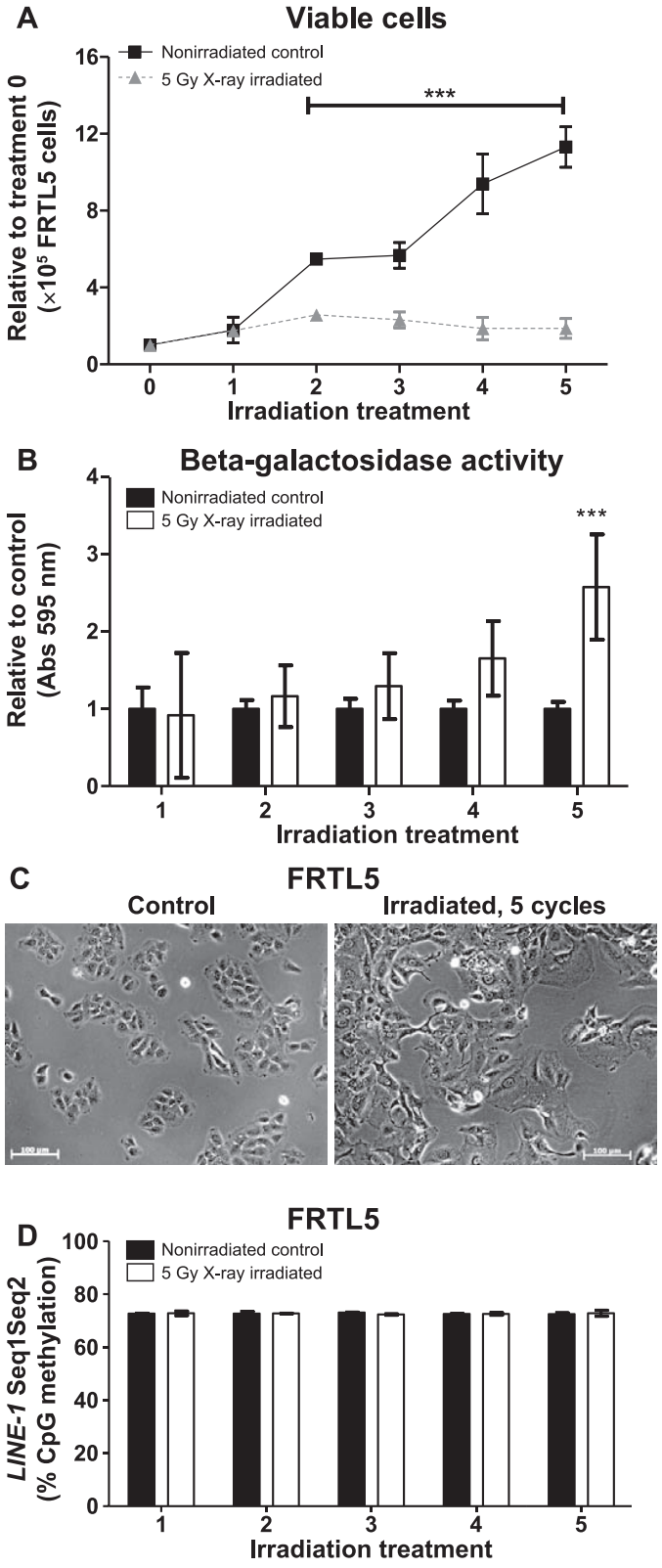

FIG. 6. Characterization of the chronic X-ray exposure model in a FRTL5 cell line. Cells received five treatments of 5 Gy with 2–3 day intervals between each exposure and assessed for cell viability (panel A), β-galactosidase activity (panel B), morphology (panel C) and *LINE-1* methylation (D). ***$P < 0.001$.

expression of this gene in FRTL5 cells. In fact, the transient inhibition of *Brca1* expression could cause premature inactivation of the mitotic checkpoint, which exerts an important role on genomic integrity, in MCF7 cells (*31*). Taking into account that *Brca1* is fundamental for homologous recombination repair (*32*), we might expect that FRTL5 cells intrinsically have less efficient DNA DSB repair machinery. Indeed, gradual loss of DNA repair genes and the accumulation of DNA damages are early steps of the carcinogenesis process in several solid tumors (*6*), including PTC (*33*).

We established a chronic radiation exposure model using the FRTL5 cell line to investigate the effects of chronic exposure on thyrocytes. In contrast to our observations with acute exposure, when FRTL5 cells were chronically exposed to radiation, a transcription activation of DNA repair genes was triggered. The striking difference between these models is that in the first one, cells maintain the capacity to proliferate, while in the latter, they become senescent. In fact, unrepaired damage and, consequently, DNA damage signaling persistence result in senescence (*34*). Evasion of senescence, in turn, could give rise to post-senescent transformed and mutated precancerous cells (*35*). Since radiation exposure is the most important risk factor for PTC (*18*), we hypothesize that there is a mechanism by which the upregulation of DNA repair machinery maintains the viability of senescent thyroid cells and, therefore, favors the accumulation of mutations that would cause cells to become susceptible to senescence evasion and transformation.

In conclusion, we report a differential HR and NHEJ gene expression in response to exposure in thyroid cells, depending on the proliferation and senescence status. Our results also suggest that intrinsic *LINE-1* hypomethylation and decreased expression of *Brca1* after acute radiation exposure, as well as the upregulation of DSB repair machinery in radiation-induced senescent cells, could lead to the accumulation of gene mutations and favor thyroid cell transformation. However, further studies are required to more fully elucidate the biological relevance of HR and NHEJ genes to thyroid carcinogenesis.

SUPPLEMENTARY INFORMATION

Fig. S1. Double-strand break repair kinetics of PCCL3. PCCL3 cells X-ray irradiated with 1, 5 and 10 Gy, and after 1, 3 and 6 h, γ-H2AX and total H2AX immunoblots were performed on nonirradiated control and irradiated cells. As a positive DSB damage control, cells were treated with 20–500 μM H_2O_2. Intensity quantification was relative to control (panel C). Beta-actin was used a loading control.

Fig. S2. Expression of HR and NHEJ genes after 10 Gy X-ray irradiation in a FRTL5 cell line. At 1–48 h postirradiation (white bars), mRNA levels of DSB DNA repair genes were evaluated. Expression levels were relative to paired nonirradiated control (black bars). *$P < 0.05$.

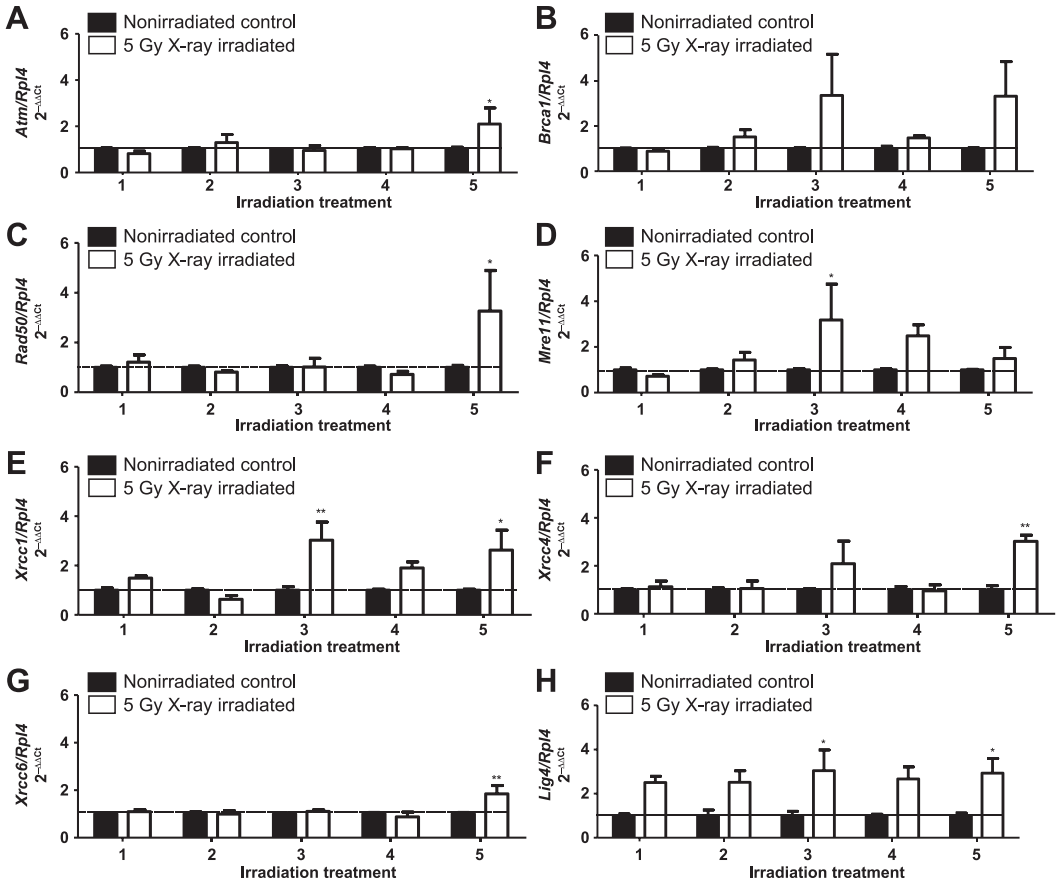

FIG. 7. HR and NHEJ gene expression in FRTL5 cell line after chronic X-ray exposure. Cells received five treatments of 5 Gy (white bars) with 2–3 h intervals between each exposure and relative mRNA expression levels according to DNA repair pathways were evaluated: HE (panels A–E) and NHEJ (panels F–H). Expression levels were relative to paired nonirradiated controls (black bars). $*P < 0.05$; $**P < 0.01$.

Table S1. Promoter methylation profiles of HR and NHEJ genes in an irradiated FRTL5 cell line. Pyrosequencing of HR (*Atm*, *Brca1*, *Rad50*, *Mre11* and *Xrcc1*) and NHEJ genes (*Xrcc4*, *Xrcc6* and *Lig4*) was performed on a 10 Gy X-ray irradiated and paired nonirradiated control FRTL5 cell line. The results were expressed as percentage of cells that displayed methylation on selected CpG sites ± SD. $*P < 0.05$ (time).

Table S2. Promoter methylation profiles of HR and NHEJ genes in a synchronized FRTL5 cell line. Pyrosequencing of HR (*Atm*, *Brca1*, *Rad50*, *Mre11* and *Xrcc1*) and NHEJ genes (*Xrcc4*, *Xrcc6* and *Lig4*) was performed on a 10 Gy X-ray irradiated and paired nonirradiated control FRTL5 cell line, previously synchronized on G_0/G_1 cell cycle phase. The results were expressed as percentage of cells that displayed methylation on selected CpG sites ± SD.

ACKNOWLEDGMENTS

This study was supported by CAPES, CNPQ and FAPERJ. AF is ''Bolsista Capes''.

Received: May 31, 2016; accepted: April 28, 2017; published online: June 2, 2017

REFERENCES

1. DeLellis RA, Lloyd RV, Heitz PU. World Health Organization Classification of Tumours. Pathology and genetics of tumours of endocrine organs. Lyon (France): IARC Press; 2004.
2. LiVolsi VA. Papillary thyroid carcinoma: an update. Mod Pathol 2011; 24:S1–9.
3. Pacini F, Vorontsova T, Demidchik EP, Molinaro E, Agate L, Romei C, et al. Post-Chernobyl thyroid carcinoma in Belarus children and adolescents: comparison with naturally occurring thyroid carcinoma in Italy and France. J Clin Endocrinol Metab 1997; 82:3563–9.
4. Caudill CM, Zhu Z, Ciampi R, Stringer JR, Nikiforov YE. Dose-dependent generation of RET/PTC in human thyroid cells after in vitro exposure to gamma-radiation: a model of carcinogenic chromosomal rearrangement induced by ionizing radiation. J Clin Endocrinol Metab 2005; 90:2364–9.
5. Grabarz A, Barascu A, Guirouilh-Barbat J, Lopez BS. Initiation of DNA double strand break repair: signaling and single-stranded resection dictate the choice between homologous recombination, non-homologous end-joining and alternative end-joining. Am J Cancer Res 2012; 2:249–68.
6. Bartkova J, Horejsí Z, Koed K, Krämer A, Tort F, Zieger K, et al. DNA damage response as a candidate anti-cancer barrier in early human tumorigenesis. Nature 2005; 434:864–70.
7. Baylin SB, Jones PA. A decade of exploring the cancer epigenome - biological and translational implications. Nat Rev Cancer 2011; 11:726–34.

8. Lima SC, Hernández-Vargas H, Simão T, Durand G, Kruel CD, Le Calvez-Kelm F, et al. Identification of a DNA methylome signature of esophageal squamous cell carcinoma and potential epigenetic biomarkers. Epigenetics 2011; 6:1217–27.
9. Weidman JR, Dolinoy DC, Murphy SK, Jirtle RL. Cancer susceptibility: epigenetic manifestation of environmental exposures. Cancer J 2007; 13:9–16.
10. Antwih DA, Gabbara KM, Lancaster WD, Ruden DM, Zielske SP. Radiation-induced epigenetic DNA methylation modification of radiation-response pathways. Epigenetics 2013; 8:839–48.
11. Ellis RJ, Wang Y, Stevenson HS, Boufraqech M, Patel D, Nilubol N, et al. Genome-wide methylation patterns in papillary thyroid cancer are distinct based on histological subtype and tumor genotype. J Clin Endocrinol Metab 2014; 99:E329–37.
12. Guan H, Ji M, Hou P, Liu Z, Wang C, Shan Z, et al. Hypermethylation of the DNA mismatch repair gene hMLH1 and its association with lymph node metastasis and T1799A BRAF mutation in patients with papillary thyroid cancer. Cancer 2008; 113:247–55.
13. Smith JA, Fan CY, Zou C, Bodenner D, Kokoska MS. Methylation status of genes in papillary thyroid carcinoma. Arch Otolaryngol Head Neck Surg 2007; 133:1006–11.
14. Agrawal N, Akbani R, Aksoy BA, Ally A, Arachchi H, Asa SL, et al. Integrated genomic characterization of papillary thyroid carcinoma. Cell 2014; 159:676–90.
15. Fusco A, Berlingieri MT, Di Fiore PP, Portella G, Grieco M, et al. One- and two-step transformations of rat thyroid epithelial cells by retroviral oncogenes. Mol Cell Biol 1987; 7:3365–70.
16. Ameziane-El-Hassani R, Boufraqech M, Lagente-Chevallier O, Weyemi U, Talbot M, Métivier D, et al. Cancer Res 2010; 70:4123–32.
17. Degrassi A, Monaco MC, Lisignoli G, Belvedere O, Toneguzzi S, Malangone W, et al. Cell cycle synchronization of FRTL5 cells. A physiological model system. J Exp Clin Cancer Res 1998; 17:527–32.
18. Ron E, Lubin JH, Shore RE, Mabuchi K, Modan B, Pottern LM, et al. Thyroid cancer after exposure to external radiation: a pooled analysis of seven studies. Radiat Res 1995; 141:259–77.
19. Hamm CA, Xie H, Costa FF, Vanin EF, Seftor EA, Sredni ST, et al. Global demethylation of rat chondrosarcoma cells after treatment with 5-aza-2′-deoxycytidine results in increased tumorigenicity. PLoS One 2009; 4:e8340.
20. Crooks GE, Hon G, Chandonia JM, Brenner SE. WebLogo: A sequence logo generator. Genome Res 2004; 14:1188–90.
21. Schmittgen TD, Livak KJ. Analyzing real-time PCR data by the comparative C(T) method. Nat Protoc 2008; 3:1101–08.
22. Nüsgen N, Goering W, Dauksa A, Biswas A, Jamil MA, Dimitriou I, et al. Inter-locus as well as intra-locus heterogeneity in LINE-1 promoter methylation in common human cancers suggests selective demethylation pressure at specific CpGs. Clin Epigenetics 2015; 7:17.
23. Green LM, Murray DK, Bant AM, Kazarians G, Moyers MF, Nelson GA, et al. Response of thyroid follicular cells to gamma irradiation compared to proton irradiation. I. Initial characterization of DNA damage, micronucleus formation, apoptosis, cell survival, and cell cycle phase redistribution. Radiat Res 2001; 155:32–42.
24. Kimura T, Van Keymeulen A, Golstein J, Fusco A, Dumont JE, Roger PP. Regulation of thyroid cell proliferation by TSH and other factors: a critical evaluation of in vitro models. Endocr Rev 2001; 22:631–56.
25. Galleani J, Miranda C, Pierotti MA, Greco A. H2AX phosphorylation and kinetics of radiation-induced DNA double strand break repair in human primary thyrocytes. Thyroid 2009; 19:257–64.
26. Maréchal A, Zou L. DNA damage sensing by the ATM and ATR kinases. Cold Spring Harb Perspect Biol 2013; 5:a012716.
27. Park SY, Seo AN, Jung HY, Gwak JM, Jung N, Cho NY, Kang GH. Alu and LINE-1 hypomethylation is associated with HER2 enriched subtype of breast cancer. PLoS One 2014; 9:e100429.
28. Kamiyama H, Suzuki K, Maeda T, Koizumi K, Miyaki Y, Okada S, et al. DNA demethylation in normal colon tissue predicts predisposition to multiple cancers. Oncogene 2012; 31:5029–37.
29. Kovalchuk O, Baulch JE. Epigenetic changes and non-targeted radiation effects – is there a link? Environ Mol Mutagen 2008; 49:16–25.
30. Dom G, Galdo VC, Tarabichi M, Tomás G, Hébrant A, Andry G, et al. 5-aza-2′-deoxycytidine has minor effects on differentiation in human thyroid cancer cell lines, but modulates genes that are involved in adaptation in vitro. Thyroid 2013; 23:317–28.
31. Chabalier C, Lamare C, Racca C, Privat M, Valette A, Larminat F. BRCA1 downregulation leads to premature inactivation of spindle checkpoint and confers paclitaxel resistance. Cell Cycle 2006; 5:1001–7.
32. Caestecker KW, Van de Walle GR. The role of BRCA1 in DNA double-strand repair: past and present. Exp Cell Res 2013; 319:575–87.
33. Leprat F, Alapetite C, Rosselli F, Ridet A, Schlumberger M, Sarasin A, et al. Impaired DNA repair as assessed by the ''comet'' assay in patients with thyroid tumors after a history of radiation therapy: a preliminary study. Int J Radiat Oncol Biol Phys 1998; 40:1019–26.
34. Klement K, Goodarzi AA. DNA double strand break responses and chromatin alterations within the aging cell. Exp Cell Res 2014; 329:42–52.
35. Nassour J, Martien S, Martin N, Deruy E, Tomellini E, Malaquin N, et al. Defective DNA single-strand break repair is responsible for senescence and neoplastic escape of epithelial cells. Nat Commun 2016; 7:10399.